Li et al. Nanoscale Research Letters (2015) 10:409
DOI 10.1186/s11671-015-1120-z

Nanoscale Research Letters
a SpringerOpen Journal

NANO EXPRESS Open Access

One-Step Synthesis of Titanium Oxyhydroxy-Fluoride Rods and Research on the Electrochemical Performance for Lithium-ion Batteries and Sodium-ion Batteries

Biao Li, Zhan Gao, Dake Wang, Qiaoyan Hao, Yan Wang, Yongkun Wang and Kaibin Tang*

Abstract

Titanium oxyhydroxy-fluoride, $TiO_{0.9}(OH)_{0.9}F_{1.2} \cdot 0.59H_2O$ rods with a hexagonal tungsten bronze (HTB) structure, was synthesized via a facile one-step solvothermal method. The structure, morphology, and component of the products were characterized by X-ray powder diffraction (XRD), thermogravimetry (TG), scanning electron microscopy (SEM), transmission electron microscopy (TEM), high-resolution TEM (HRTEM), inductively coupled plasma optical emission spectroscopy (ICP-OES), ion chromatograph, energy-dispersive X-ray (EDX) analyses, and so on. Different rod morphologies which ranged from nanoscale to submicron scale were simply obtained by adjusting reaction conditions. With one-dimension channels for Li/Na intercalation/de-intercalation, the electrochemical performance of titanium oxyhydroxy-fluoride for both lithium-ion batteries (LIBs) and sodium-ion batteries (SIBs) was also studied. Electrochemical tests revealed that, for LIBs, titanium oxyhydroxy-fluoride exhibited a stabilized reversible capacity of 200 mAh g^{-1} at 25 mA g^{-1} up to 120 cycles in the electrode potential range of 3.0–1.2 V and 140 mAh g^{-1} at 250 mA g^{-1} up to 500 cycles, especially; for SIBs, a high capacity of 100 mAh g^{-1} was maintained at 25 mA g^{-1} after 115 cycles in the potential range of 2.9–0.5 V.

Keywords: Lithium-ion batteries; Sodium-ion batteries; Metal oxyhydroxy-fluoride; Hexagonal tungsten bronze; Solvothermal method

Background

Mixed-anion metal fluorides, which include metal oxyhydroxy-fluorides, metal hydroxy-fluorides, metal oxyfluorides, and so on, have become more and more attractive because of their characteristic structures and properties [1–12]. For example, $FeOF_{1-x}(OH)_x \cdot nH_2O$ adopted the α-MnO_2 structure [3], $Ti_{0.75}(OH)_{1.5}F_{1.5}$ with the ReO_3-type structure was studied as a UV absorber [8], and $Ce_{1-x}Ca_xO_{2-x-y/2}F_y$ with the fluorite-type structure exhibited UV-shielding property [10]. In recent years, to extend the scope of existing electrode materials for lithium-ion batteries (LIBs) as well as sodium-ion batteries (SIBs) and make more progress in the development of clean energy, the use of mixed-anion metal fluorides was more and more popular [5, 13–24]. Iron-based fluorides with the hexagonal tungsten bronze (HTB) structure were regarded as potential candidates for cathode material, and the research on their electrochemical performance has been ongoing for a period of time [5, 13]. Demourgues et al. reported that $FeF_{2.2}(OH)_{0.8-y}O_{y/2}\square_{y/2}$ with the HTB structure displayed better cyclability and reversible capacity than the precursor $FeF_{2.2}(OH)_{0.8} \cdot (H_2O)_{0.33}$ for LIBs [5]. Wang et al. reported that $FeF_3 \cdot xH_2O$ including the HTB structure $FeF_3 \cdot 0.33H_2O$ exhibited a discharge capacity of 101 mAh g^{-1} after 30 cycles in the potential range of 4.0–1.0 V at 0.1 C, which was quite high for SIBs [13]. Importantly, the electrochemical characteristics of the original samples proved the potentiality for further research.

In fact, another metal oxyhydroxy-fluoride with the HTB structure, titanium oxyhydroxy-fluoride has been reported by Demourgues et al. [2]. With the same one-dimension channels in structure and lighter Ti atomic weight, titanium oxyhydroxy-fluoride is also considered to be an attractive electrode material which supports Li/Na

* Correspondence: kbtang@ustc.edu.cn
Department of Chemistry and Hefei National Laboratory for Physical Science at Microscale, University of Science and Technology of China, Hefei, Anhui 230026, People's Republic of China

intercalation/de-intercalation into the host structure. The electrochemical reaction is supposed to benefit keeping certain electrode potential and studying how the HTB structure influences the electrochemical properties.

Herein, we demonstrate a facile one-step method to synthesize titanium oxyhydroxy-fluoride rods by introducing anions into titanium binary fluoride. The synthesis route started with the use of TiF_4 powder (fluorine source), ethanol, and deionized water. The deionized water and ethanol volume using in reaction played significant roles in controlling the structure and morphology of the products, respectively. Structure features were studied by analyses of X-ray powder diffraction (XRD), thermogravimetry (TG), high-resolution TEM (HRTEM), and so on. Besides, the electrochemical properties of as-prepared half-cells were evaluated in detail for both LIBs and SIBs, which may help shed new light on the Li/Na intercalation/de-intercalation mechanism.

Methods

Preparation

Titanium oxyhydroxy-fluoride was prepared as follows: TiF_4 (Alfa Aesar 98 %) was firstly ground to fine powder in a glove box. After that, 1 g TiF_4 was taken out and put in a 10 mL Teflon autoclave, then 1.20 mL deionized water and a certain volume of ethanol were put in the autoclave sequentially. Operation in this step should be quick to avoid earlier hydrolysis of TiF_4. The autoclave was heated to 150 °C and kept for 48 h. The precipitate was centrifuged, washed with deionized water over three times, and kept in a vacuum oven at 60 °C for 12 h to get the final products. The ethanol volume used can be described as follows: 1.88 mL ethanol for long titanium oxyhydroxy-fluoride rods, 0.47 mL ethanol for short titanium oxyhydroxy-fluoride rods, and 0.94 mL ethanol for titanium oxyhydroxy-fluoride with the morphology of hexagonal rods. In this article, the sample used for TG and galvanostatic charge–discharge tests is long $TiO_{0.9}(OH)_{0.9}F_{1.2} \cdot 0.59H_2O$ rods.

Characterization

The crystal structure features of as-prepared materials were characterized by X-ray powder diffraction on a Philips X'pert X-ray diffractometer using Cu Kα1 radiation at room temperature. The morphology images of as-prepared materials were taken on a JEOL JSM-6700F scanning electron microscope. The transmission electron microscopy (TEM) and HRTEM images were taken on a JEOL-2010 transmission electron microscope. The thermostabilization of as-prepared materials was characterized by thermogravimetry analysis on a DTG-60H thermogravimetry analyzer which worked under nitrogen atmosphere at a heating rate of 10 °C/min from room temperature to 700 °C. The Ti content was characterized by inductively coupled plasma optical emission spectroscopy (ICP-OES) using Atomscan Advantage. The F content was characterized by ion chromatograph (ICS-3000). The [F]/[Ti] molar ratio was further confirmed by energy-dispersive X-ray (EDX) analysis recorded on the JEOL-2010 transmission electron microscope.

Electrochemical Measurement

The electrochemical behavior of all the aforementioned products was tested for LIBs and SIBs by the galvanostatic charge–discharge method at room temperature. For LIBs, the half-cells were composed of the as-prepared product as working electrode, Li metal as counter and reference electrode, and the 1 M $LiPF_6$ ethylene carbonate/dimethylcarbonate (volume ratio 1:1) solution as electrolyte, which were assembled as coin cells (2016 R-type). The composition of the working electrode was active material (70 %), Super P-carbon black (20 %), and sodium carboxymethyl cellulose binder (10 %); 70, 20 and 10 % were the weight percentage. The above mixture was ground in water and then homogeneously pasted on a Cu slice; after that, the Cu slice was dried in a vacuum oven which was heated to 80 °C for 12 h. The assembling was operated in a glove box. The glove box was full of argon, in which oxygen and H_2O were kept under 0.1 ppm. For SIBs, the preparation of Cu slice with the active material was in the same procedure which has been introduced above. The differences were we used Na metal as counter and reference electrode, fiberglass instead of polypropylene as separator, and 1 M $NaClO_4$ in propylene carbonate as electrolyte. Tests of electrochemical performance were taken on a Neware-BTS-TC53 instrument at required current densities and in the appropriate electrode potential window.

Results and Discussion

The XRD pattern of titanium oxyhydroxy-fluoride is shown in Fig. 1. All of the diffraction peaks are indexed by a hexagonal lattice with the lattice parameters a = 7.3636 Å, c = 7.5186 Å, and the space group $P6_3/mmc$, which are consistent with the HTB-$Ti_{0.75}O_{0.25}(OH)_{1.3}F_{1.2}$ reported by Demourgues et al. [2]. It is confirmed that titanium oxyhydroxy-fluoride had the HTB structure without observed impurity. The atom mole ratio [F]/[Ti] is 1.2 which is confirmed by analyzing the results of ion chromatograph, ICP-OES, and EDX. The HTB structural frame shown as inlet is viewed down the [001] direction; the one-dimension channels in the structure are expected to benefit Li and Na intercalation/de-intercalation. It is noteworthy that, the XRD patterns of titanium oxyhydroxy-fluoride with different morphologies are identical.

TG curves of titanium oxyhydroxy-fluoride are shown in Fig. 2. There are two weight losses in the thermal decomposition of titanium oxyhydroxy-fluoride from room

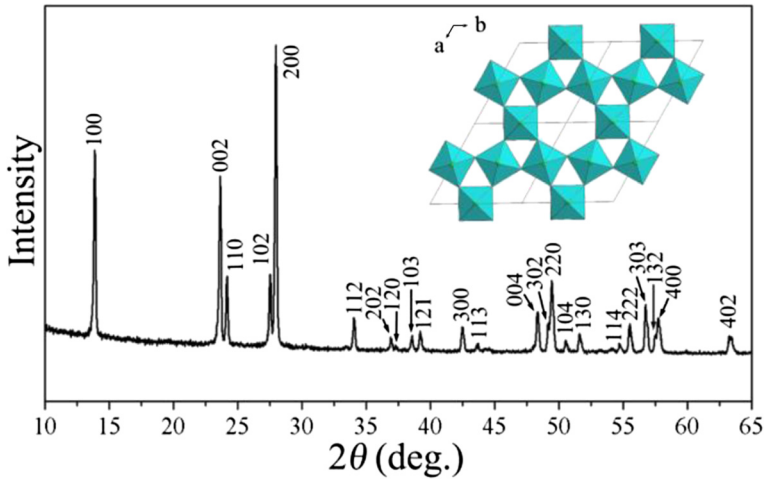

Fig. 1 XRD pattern of titanium oxyhydroxy-fluoride. The HTB structural frame is shown as inlet

temperature to 700 °C. Firstly, a weight loss of approx 9 % occurs and ends at 370 °C. It is considered that the first weight loss is related to the water absorbed on titanium oxyhydroxy-fluoride powders. Secondly, a bulky weight loss of 41 % occurring at 370–520 °C is considered to be due to the thermal decomposition of titanium oxyhydroxy-fluoride. In this period, OH and F constituents depart in the form of H_2O and TiF_4 (g), respectively. It can also be considered that the sequential H_2O departure and TiF_4 loss correspond to the two peaks of the first derivative, for the fact under certain temperature only H_2O departure is observed in the thermal treatment of $FeF_{2.2}(OH)_{0.8} \cdot (H_2O)_{0.33}$ which is reported by Demourgues et al. [5]. The thermal decomposition of titanium oxyhydroxy-fluoride finally leads to the formation of TiO_2 when the temperature reaches 520 °C. The bulky weight loss and decomposition temperature of titanium oxyhydroxy-fluoride are similar to $TiOF_2$ which has been studied recently [16, 25]. After taking into consideration of the analyses of the TG curves and the mole ratio [F]/[Ti], the formula for titanium oxyhydroxy-fluoride should be proposed as: $TiO_{0.9}(OH)_{0.9}F_{1.2} \cdot 0.59H_2O$, which is analogous to the one presented by Demourgues et al. [2].

The morphology and structure features of titanium oxyhydroxy-fluoride, $TiO_{0.9}(OH)_{0.9}F_{1.2} \cdot 0.59H_2O$ particles are also investigated through the analyses of scanning electron microscopy (SEM), TEM, HRTEM images and the corresponding FFT image. The size of long $TiO_{0.9}(OH)_{0.9}F_{1.2} \cdot 0.59H_2O$ rods (Fig. 3a) is approx 2 μm long and 100–500 nm in diameter; the typical long rod with the regular shape is shown in Fig. 3d. For short $TiO_{0.9}(OH)_{0.9}F_{1.2} \cdot 0.59H_2O$ rods (Fig. 3b), the length ranges from 700 to 1300 nm and the diameter ranges

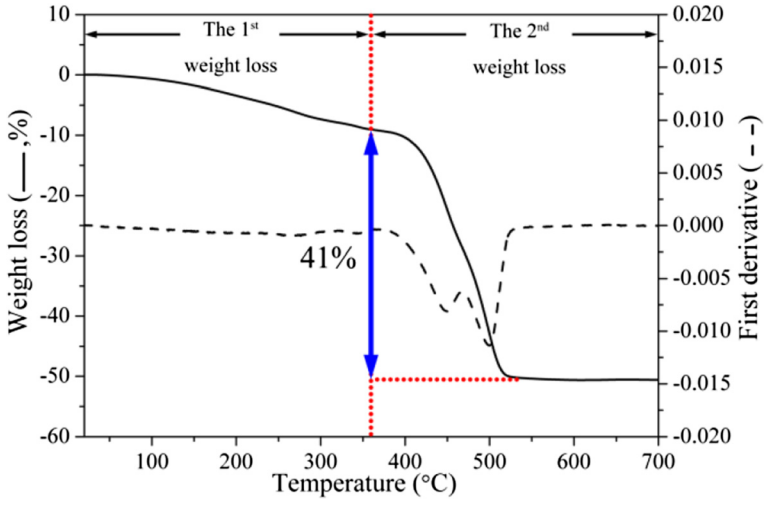

Fig. 2 TG curves of titanium oxyhydroxy-fluoride

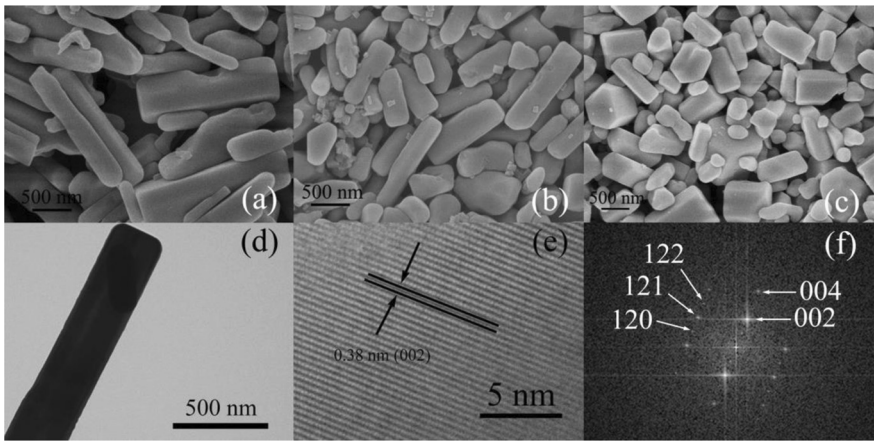

Fig. 3 SEM images of titanium oxyhydroxy-fluoride, $TiO_{0.9}(OH)_{0.9}F_{1.2} \cdot 0.59H_2O$ with different morphologies: long rods (**a**), short rods (**b**) and hexagonal rods (**c**); TEM image (**d**), HRTEM image (**e**) and the corresponding FFT image (**f**) of long $TiO_{0.9}(OH)_{0.9}F_{1.2} \cdot 0.59H_2O$ rods; the arrows in the HRTEM image (**e**) indicate the 0.38 nm interfringe spacing, and the arrows in the corresponding FFT image (**f**) indicate the spots which represent different lattice planes of the product

from 250 to 400 nm. All the $TiO_{0.9}(OH)_{0.9}F_{1.2} \cdot 0.59H_2O$ rods with different morphologies are synthesized under the same condition with the only difference of the ethanol volume. Actually, if only the volume of deionized water is changed (from 1.20 mL to 0.15 mL), another compound hexagonal $TiOF_2$ is synthesized. The sole difference between the synthesis of $TiO_{0.9}(OH)_{0.9}F_{1.2} \cdot 0.59H_2O$ and hexagonal $TiOF_2$,i.e., the volume of deionized water indicates that during the synthesis of $TiO_{0.9}(OH)_{0.9}F_{1.2} \cdot 0.59H_2O$, more hydrolysis reactions of TiF_4 occur and Ti^{4+} binds the generated hydroxy to form the final product with the HTB structure. In other words, the hydroxy groups are considered to be very important for the firm HTB structure. It can also be concluded that the deionized water volume of reaction decides the structure of the products while the ethanol volume plays a significant role in affecting the morphology. The 0.38-nm interfringe spacing in

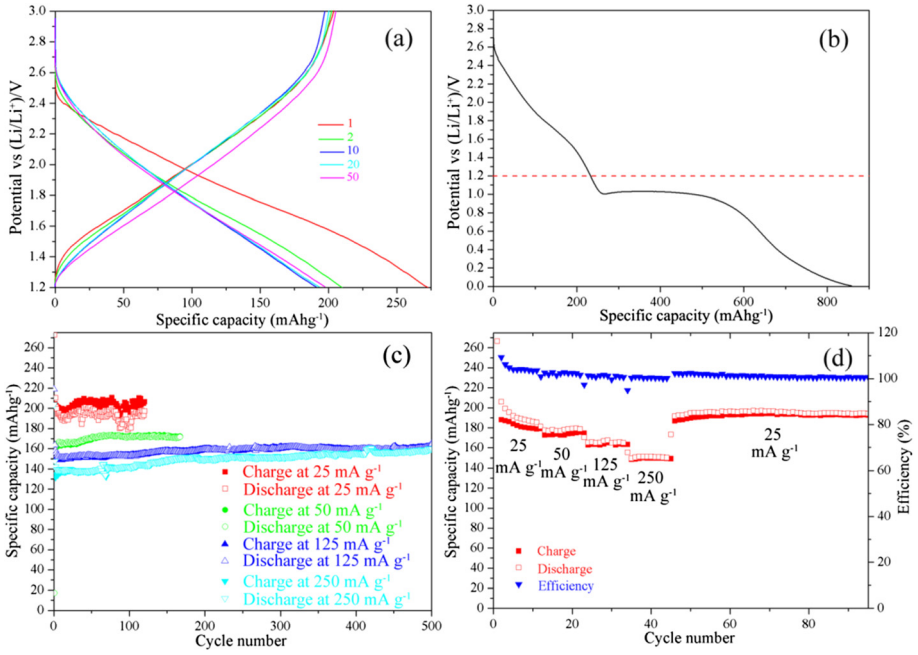

Fig. 4 **a** Charge and discharge curves of $TiO_{0.9}(OH)_{0.9}F_{1.2} \cdot 0.59H_2O$ for LIBs, the half-cell is performed at 25 mA g^{-1}; several selected cycles are shown for clarity; **b** first discharge curve of $TiO_{0.9}(OH)_{0.9}F_{1.2} \cdot 0.59H_2O$ which is performed at 25 mA g^{-1} in the potential range of 3.0–0.05 V; **c** cycling performance of $TiO_{0.9}(OH)_{0.9}F_{1.2} \cdot 0.59H_2O$; and **d** rate capacity of one $TiO_{0.9}(OH)_{0.9}F_{1.2} \cdot 0.59H_2O$ half-cell for LIBs between 3.0–1.2 V, different current densities are labeled

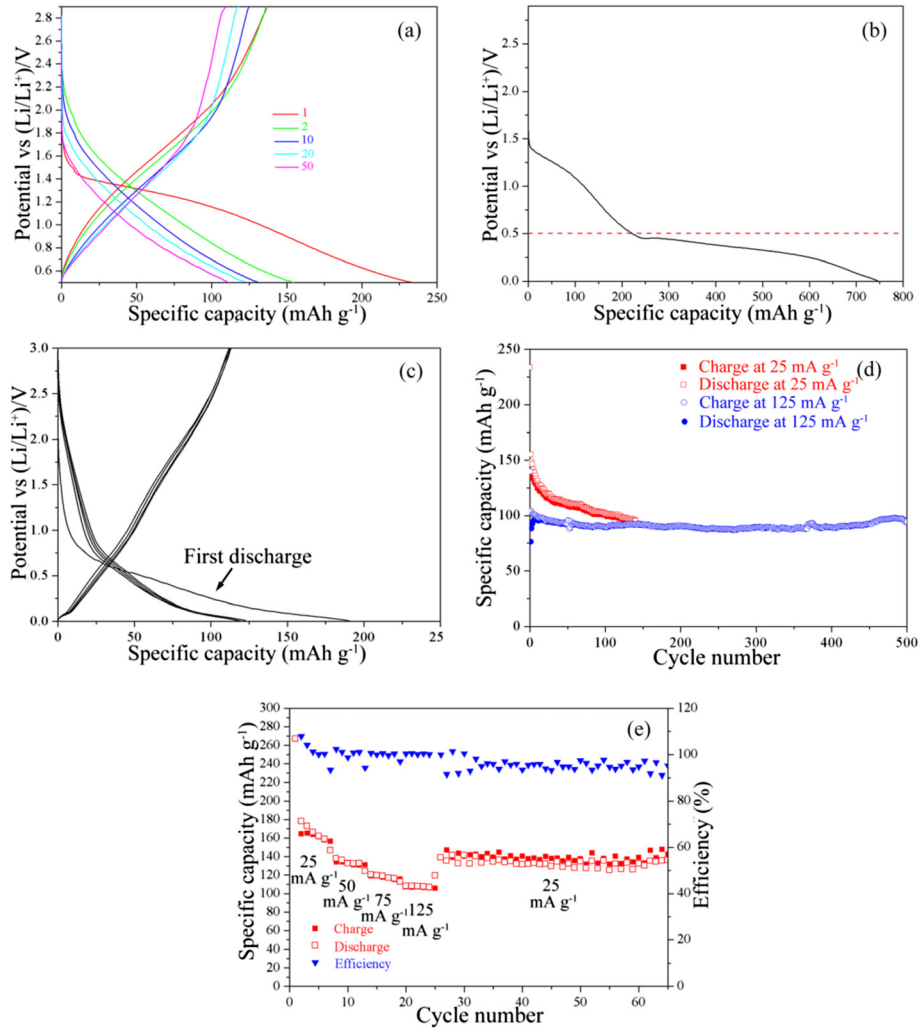

Fig. 5 a Charge and discharge curves of $TiO_{0.9}(OH)_{0.9}F_{1.2} \cdot 0.59H_2O$ for SIBs in the potential range of 2.9–0.5 V; several selected cycles are shown for clarity; **b** first discharge curve of $TiO_{0.9}(OH)_{0.9}F_{1.2} \cdot 0.59H_2O$ in the potential range of 2.9–0.05 V; **c** the former 5 cycles of hexagonal $TiOF_2$ half-cell for SIBs; all the half-cells are performed at 25 mA g^{-1}; **d** cycling performance of $TiO_{0.9}(OH)_{0.9}F_{1.2} \cdot 0.59H_2O$ for SIBs; and **e** rate capacity of one $TiO_{0.9}(OH)_{0.9}F_{1.2} \cdot 0.59H_2O$ half-cell for SIBs between 2.9 and 0.5 V, different current densities are labeled

Fig. 3e corresponds to the (002) lattice plane of $TiO_{0.9}(OH)_{0.9}F_{1.2} \cdot 0.59H_2O$. The vertical (120) and (002) lattice plane in Fig. 3e are also confirmed by the FFT image (Fig. 3f).

To investigate the electrochemical properties of titanium oxyhydroxy-fluoride $TiO_{0.9}(OH)_{0.9}F_{1.2} \cdot 0.59H_2O$, both LIBs and SIBs are performed by using galvanostatic charge/discharge method. The results are shown in Figs. 4 and 5. For LIBs, during the first cycle, the discharge plateau appears at 2.4 V and last until the electrode potential reaches 1.2 V, and the only one plateau suggests that there is only one lithiated $TiO_{0.9}(OH)_{0.9}F_{1.2} \cdot 0.59H_2O$ phase ,i.e., no other phase transition of $TiO_{0.9}(OH)_{0.9}F_{1.2} \cdot 0.59H_2O$ is observed during the lithiation of $TiO_{0.9}(OH)_{0.9}F_{1.2} \cdot 0.59H_2O$. The potential range where Li intercalation/de-intercalation occurs in is 3.0–1.2 V, which can also be illustrated by Fig. 4b. The specific capacity of the first discharge and the first charge is 270 mAh g^{-1} and 200 mAh g^{-1}, while the specific capacities of the following cycles, whether of charge or of discharge, are approx 200 mAh g^{-1}. $TiO_{0.9}(OH)_{0.9}F_{1.2} \cdot 0.59H_2O$ exhibits stabilized 200, 170, 150, and 140 mAh g^{-1} at 25, 50, 125, and 250 mA g^{-1}, respectively, in the electrode potential range of 3–1.2 V without observed fading for 120–500 cycles (Fig. 4c and d), which is pretty satisfying and illustrates the highly reversible nature. Besides, after cycling at 25 mA g^{-1} again, the specific capacity of $TiO_{0.9}(OH)_{0.9}F_{1.2} \cdot 0.59H_2O$ is recovered (Fig. 4d). It is noteworthy that the stabilized 200 mAh g^{-1} capacity of $TiO_{0.9}(OH)_{0.9}F_{1.2} \cdot 0.59H_2O$ is quite large, compared with that of $Li_4Ti_5O_{12}$ (theoretical capacity 170 mAh g^{-1}). The good rate capacity and cycling stability are connected

with the one-dimension channels in the HTB structure and the morphology of homogeneous rods.

For SIBs, in the first cycle the discharge plateau appears at about 1.6 V and ends at 0.5 V which is higher than TiO_2 [26], and the potential of Na intercalation/de-intercalation is above 0.5 V which is shown in Fig. 5b. The specific capacity of the first discharge is 233 mAh g^{-1} (Fig. 5a), and after the first discharge, the specific capacity gradually decreases from 150 mAh g^{-1} (the second discharge) to 111 mAh g^{-1} (the 50th discharge), but it is still above 100 mAh g^{-1} after 115 cycles (Fig. 5d). The electrochemical performance of another product obtained under the similar reaction condition, hexagonal $TiOF_2$, is shown in Fig. 5c, the details of this work is introduced in another article which is submitting. The capacities of the former 20 cycles of the $TiO_{0.9}(OH)_{0.9}F_{1.2} \cdot 0.59H_2O$ half-cell in the potential range of 2.9–0.5 V are higher than hexagonal $TiOF_2$ even the potential ranges from 3.0 to 0.05 V, which is considered to be facilitated by the HTB structure. The $TiO_{0.9}(OH)_{0.9}F_{1.2} \cdot 0.59H_2O$ half-cell cycled at 125 mA g^{-1} stabilizes at a specific capacity of 100 mAh g^{-1} and it is considered to be due to the incomplete Na intercalation/de-intercalation (Fig. 5d). The rate capacity of $TiO_{0.9}(OH)_{0.9}F_{1.2} \cdot 0.59H_2O$ for SIBs is shown in Fig. 5e, $TiO_{0.9}(OH)_{0.9}F_{1.2} \cdot 0.59H_2O$ exhibits a capacity of 160, 130, 120, and 100 mAh g^{-1} cycled at 25, 50, 75, and 125 mA g^{-1}, respectively. 76 % capacity of the second discharge ,i.e., 130 mAh g^{-1} is retained after cycling at 25 mA g^{-1} again without observed fading for another 35 cycles. Compared with LIBs, the electrochemical performance of $TiO_{0.9}(OH)_{0.9}F_{1.2} \cdot 0.59H_2O$ for SIBs is restricted, whether the capacities or the cycling stability, which may be related to the different ion sizes and diffusion rates of Li and Na ions.

Conclusions

In summary, titanium oxyhydroxy-fluoride $TiO_{0.9}(OH)_{0.9}F_{1.2} \cdot 0.59H_2O$ with the HTB structure is synthesized by a facile one-step method. The purity of the products is confirmed, and products with various morphologies are obtained by adjusting the volume of ethanol used in the synthesis process. The electrochemical performance of $TiO_{0.9}(OH)_{0.9}F_{1.2} \cdot 0.59H_2O$ is also studied to investigate Li/Na intercalation/de-intercalation in the HTB structure. For LIBs, $TiO_{0.9}(OH)_{0.9}F_{1.2} \cdot 0.59H_2O$ delivered a stabilized capacity of 200 mAh g^{-1} under a current density of 25 mA g^{-1} in the former 120 cycles; the capacities of 150 mAh g^{-1} and 140 mAh g^{-1} are also exhibited without observed fading after 500 cycles at 125 mA g^{-1} and 250 mA g^{-1}, respectively, which demonstrated the highly reversible cycling stability of $TiO_{0.9}(OH)_{0.9}F_{1.2} \cdot 0.59H_2O$. For SIBs, $TiO_{0.9}(OH)_{0.9}F_{1.2} \cdot 0.59H_2O$ exhibits capacities above 130 mAh g^{-1} in the former 20 cycles and capacities above 100 mAh g^{-1} in the former 115 cycles, which is quite large and it is potential for the further improvement of $TiO_{0.9}(OH)_{0.9}F_{1.2} \cdot 0.59H_2O$. We believe $TiO_{0.9}(OH)_{0.9}F_{1.2} \cdot 0.59H_2O$ is potential as an electrode material, and the electrochemical properties will be improved by further research such as nanocomposite and carbon-coated process.

Competing Interests

The authors declare that they have no competing interests.

Authors' Contributions

BL and KT designed the experiment. BL, ZG, and DW carried out the experiment. BL and QH participated in the cell fabrication. BL wrote the manuscript. BL and YW analyzed the XRD data and electrochemical properties of the electrodes. YKW and KT gave important advices on the draft manuscript and finalized the manuscript. All authors examined and approved the final manuscript.

Acknowledgements

This work was supported by the National Natural Science Foundation of China (no. 21171158) and National Basic Research Program of China (2010CB934700).

Received: 10 September 2015 Accepted: 12 October 2015
Published online: 17 October 2015

References

1. Demourgues A, Francke L, Durand E, Tressaud A (2002) Chemistry and key structural features of oxyhydroxy-fluorides: relationships with the acidic character, thermal stability and surface area. J Fluorine Chem 114(2):229–236
2. Demourgues A, Penin N, Dambournet D, Clarenc R, Tressaud A, Durand E (2012) About MX3 and MX2 (Mn+ = Mg2+, Al3+, Ti4+, Fe3+; Xp– = F–, O2–, OH–) nanofluorides. J Fluorine Chem 134:35–43. doi:10.1016/j.jfluchem.2011.02.006
3. Demourgues A, Wattiaux A (2011) Investigation of Fe-based oxyhydroxy-fluoride with hollandite-type structure. J Fluorine Chem 132(10):690–697. doi:10.1016/j.jfluchem.2011.04.005
4. Estruga M, Casas-Cabanas M, Gutiérrez-Tauste D, Domingo C, Ayllón JA (2010) Straightforward synthesis of a novel hydronium titanium oxyfluoride. Mater Chem Phys 124(2–3):904–907. doi:10.1016/j.matchemphys.2010.08.008
5. Duttine M, Dambournet D, Penin N, Carlier D, Bourgeois L, Wattiaux A , Chapman KW, Chupas PJ, Groult H, Durand E, Demourgues A (2014) Tailoring the composition of a mixed anion iron-based fluoride compound: evidence for anionic vacancy and electrochemical performance in lithium cells. Chem Mater 26(14):4190–4199. doi:10.1021/cm501396n
6. Dambournet D, Chapman KW, Chupas PJ, Gerald RE 2nd, Penin N, Labrugere C, Demourgues A, Tressaud A, Amine K (2011) Dual lithium insertion and conversion mechanisms in a titanium-based mixed-anion nanocomposite. J Am Chem Soc 133(34):13240–13243. doi:10.1021/ja204284h
7. Francke LC, Durand E, Demourgues A, Vimont A, Daturi M, Tressaud A (2003) Synthesis and characterization of Al3+, Cr3+, Fe3+ and Ga3+ hydroxyfluorides: correlations between structural features, thermal stability and acidic properties. J Mater Chem 13(9):2330. doi:10.1039/b303535b
8. Demourgues A, Penin N, Durand E, Weill F, Dambournet D, Viadère N, Tressaud A (2009) New titanium hydroxyfluoride Ti0.75(OH)1.5F1.5 as a UV absorber. Chem Mater 21(7):1275–1283
9. Dejneka MJ (1998) The luminescence and structure of novel transparent oxyfluoride glass-ceramics. J Non-Cryst Solids 239(1):149–155
10. Sronek L, Majimel J, Kihn Y, Montardi Y, Tressaud A, Feist M, Legein C, Buzaré JY, Body M, Demourgues A (2007) New highly divided Ce-Ca-based oxyfluorides with UV-shielding properties: study of the Ce1-xCaxO2-x and Ce1-xCaxO2-x-y/2Fy series. Chem Mater 19(21):5110–5121
11. Lin H, Maggard PA (2010) Microporosity, optical bandgap sizes, and photocatalytic activity of M(I)-Nb(V) (M = Cu, Ag) Oxyfluoride Hybrids. Cryst Growth Des 10(3):1323–1331. doi:10.1021/cg9013625
12. Wang J, Cao F, Bian Z, Leung MK, Li H (2014) Ultrafine single-crystal TiOF2 nanocubes with mesoporous structure, high activity and durability in visible light driven photocatalysis. Nanoscale 6(2):897–902. doi:10.1039/c3nr04489k
13. Shen Y, Wang X, Hu H, Jiang M, Yang X, Shu H (2015) A graphene loading heterogeneous hydrated forms iron based fluoride nanocomposite as novel

and high-capacity cathode material for lithium/sodium ion batteries. J Power Sources 283:204–210. doi:10.1016/j.jpowsour.2015.02.097
14. Reddy MV, Madhavi S, Subba Rao GV, Chowdari BVR (2006) Metal oxyfluorides TiOF2 and NbO2F as anodes for Li-ion batteries. J Power Sources 162(2):1312–1321. doi:10.1016/j.jpowsour.2006.08.020
15. Deng D, Kim MG, Lee JY, Cho J (2009) Green energy storage materials: nanostructured TiO2 and Sn-based anodes for lithium-ion batteries. Energy Environ Sci 2(8):818. doi:10.1039/b823474d
16. Louvain N, Karkar Z, El-Ghozzi M, Bonnet P, Guerin K, Willmann P (2014) Fluorination of anatase TiO2 towards titanium oxyfluoride TiOF2: a novel synthesis approach and proof of the Li-insertion mechanism. J Mater Chem A 2(37):15308–15315. doi:10.1039/C4TA02553A
17. Zeng Y, Zhang W, Xu C, Xiao N, Huang Y, Yu DY, Hng HH, Yan Q (2012) One-step solvothermal synthesis of single-crystalline TiOF2 nanotubes with high lithium-ion battery performance. Chemistry 18(13):4026–4030. doi:10.1002/chem.201103879
18. Pereira N, Badway F, Wartelsky M, Gunn S, Amatucci GG (2009) Iron oxyfluorides as high capacity cathode materials for lithium batteries. J Electrochem Soc 156(6):A407. doi:10.1149/1.3106132
19. Gocheva ID, Tanaka I, Doi T, Okada S, Yamaki J-I (2009) A new iron oxyfluoride cathode active material for Li-ion battery, Fe2OF4. Electrochem Commun 11(8):1583–1585. doi:10.1016/j.elecom.2009.06.001
20. Hamwi A, Al Saleh I (1994) Graphite oxyfluoride: behaviour as electrode material in lithium batteries. J Power Sources 48(3):311–325, http://dx.doi.org/10.1016/0378-7753(94)80028-6
21. Choi W, Manthiram A (2007) Influence of fluorine substitution on the electrochemical performance of 3 V spinel Li4Mn5O12 – ηFη cathodes. Solid State Ionics 178(27–28):1541–1545. doi:10.1016/j.ssi.2007.10.003
22. Bervas M, Klein LC, Amatucci GG (2006) Reversible conversion reactions with lithium in bismuth oxyfluoride nanocomposites. J Electrochem Soc 153(1):A159. doi:10.1149/1.2133712
23. Amatucci GG, Pereira N (2007) Fluoride based electrode materials for advanced energy storage devices. J Fluorine Chem 128(4):243–262. doi:10.1016/j.jfluchem.2006.11.016
24. Zhu J, Deng D (2015) Wet-chemical synthesis of phase-pure FeOF nanorods as high-capacity cathodes for sodium-ion batteries. Angew Chem Int Ed 54(10):3079–3083. doi:10.1002/anie.201410572
25. Xie S, Han X, Kuang Q, Fu J, Zhang L, Xie Z, Zheng L (2011) Solid state precursor strategy for synthesizing hollow TiO2 boxes with a high percentage of reactive {001} facets exposed. Chem Commun (Camb) 47(23):6722–6724. doi:10.1039/c1cc11542a
26. Bi Z, Paranthaman MP, Menchhofer PA, Dehoff RR, Bridges CA, Chi M, Guo B, Sun XG, Dai S (2013) Self-organized amorphous TiO2 nanotube arrays on porous Ti foam for rechargeable lithium and sodium ion batteries. J Power Sources 222:461–466. doi:10.1016/j.jpowsour.2012.09.019